Journal of Computer Science and Cybernetics, V.40, N.2 (2024), 135–146
DOI no. 10.15625/1813-9663/18655

A NEW METHOD FOR MEDICAL IMAGE FUSION BASED ON GAUSSIAN BLUR FILTER AND ROBINSON COMPASS OPERATOR

QUOC VIET KIEU[1], VINH NAM HUYNH[1], THI PHUONG NGHIEM[1], OANH CUONG DO[1,2], GIANG SON TRAN[1,*]

[1]*ICTLab, University of Science and Technology of Hanoi, Vietnam Academy of Science and Technology, 18 Hoang Quoc Viet Street, Cau Giay District, Ha Noi, Viet Nam*
[2]*Faculty of Computer Science and Engineering, Thuyloi University, 175 Tay Son Street, Dong Da District, Ha Noi, Viet Nam*

Abstract. Medical image fusion is a process of extracting features from multi-modal medical images and combining them into a composite image. It brings huge support in medical imaging and clinical diagnosis. However, the extraction of both structural and functional information from input MRI and PET images using multi-scale transform fusion methods poses a challenge of providing high-quality decomposition layers since during the decomposition process, images can still lose information such as blur or noise at the edges of the image. To address this limitation, we present a new method to improve the visual information fidelity of medical image fusion. Firstly, the YCbCr color space is utilized to prevent distortion when merging color and grey images. The second algorithm uses the CLAHE model, which allows the input images to have good contrast. Then, a Gaussian blur filter is employed to decompose the images into base and detail layers. The use of Gaussian blur ensures a smoothing filter of the edges. After that, the Robinson compass operator is applied to create the fusion rule of detail components. Finally, the fused base and detail layers are concatenated together to form the final composite image. The experimental results show that the proposed approach outperforms the latest methods in bringing visual information fidelity of the input images to the fused image, which is helpful in supporting doctors and radiologists in visual analysis of the medical images.

Keywords. Medical image fusion, two-scale image decomposition, Gaussian blur filter, compass operator.

1. INTRODUCTION

In medical imaging, fusion is a common technique to extract features from multi-modal images and combine them into one image. Medical image fusion includes various modalities: Single photon emission computed tomography (SPECT), Positron emission tomography (PET), Magnetic resonance imaging (MRI), and Computed tomography (CT). Each type of image modality has its own features and specific information for radiologists to use in

*Corresponding author.
E-mail addresses: kieu-quoc.viet@usth.edu.vn (Q.V. Kieu); huynh-vinh.nam@usth.edu.vn (V.N. Huynh); nghiem-thi.phuong@usth.edu.vn (N.T. Phuong); cuongdo@tlu.edu.vn (O.C. Do); tran-giang.son@usth.edu.vn (G.S. Tran);

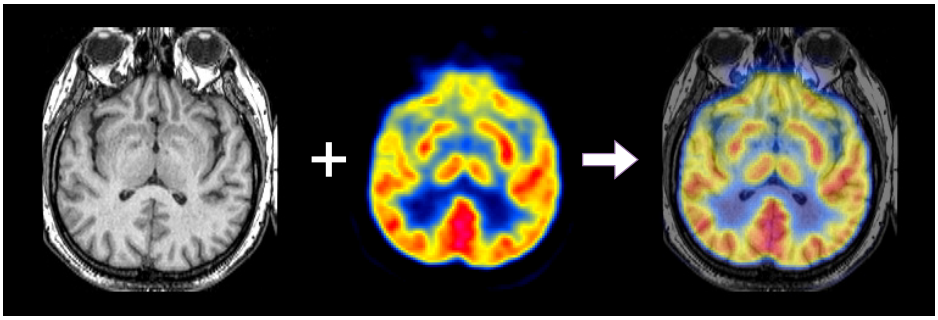

Figure 1: Example of multi-modal medical image fusion: An MRI image (left) is fused with a PET image (middle) to form an MRI/PET composite image (right).

diagnosing diseases [1]. For example, SPECT images allow radiologists to examine perfusion and functionality in color, low-resolution images. Meanwhile, MRI images offer anatomical and structural information in grayscale and high resolution. Fig. 1 illustrates an example of a composite MRI/PET image (right) which combines an MRI image (left) with a PET image (middle).

Currently, there are two main categories for medical image fusion: spatial-domain methods and transform-domain ones [2]. In the first category, the input images are processed in the spatial domain. The processing tasks can be on as small scale as pixels [3], areas, or even as large as a whole part of the image [4] with various fusion rules such as maximum/minimum selection or weighted average rules. The main advantage of the spatial-domain approaches is that they supply spatial information of the input images for the fusion process. However, the fused image can lose information because of the lack of spectral information in those methods.

In the second category, the input images are processed in the transformed domain. To do so, they are first converted from the spatial domain to the transform domain by using some transformation techniques. Then, the transform coefficients are fused together using certain fusion rules. Finally, an inverse transformation is applied to produce the output composite image. In those approaches, many transform methods can be used such as Laplacian Pyramid [5, 6], Contourlet Transform [7], Shearlet Transform [8], Fast Fourier transform (FFT) [9, 10], and Discrete wavelet transform (DWT) [11, 12]. The transformation can be a two-scale transform as in [9, 10, 13] or a multi-scale transform as in [14, 15]. After the transform step, many techniques are proposed to create the fusion rules in the transform domain. For example, in [9, 10, 16, 17], the authors employ meta-heuristic optimization algorithms and maximum local energy functions to create fusion rules for detail and base features. Besides, in [18, 19], the authors utilize deep learning-based transfer learning techniques for medical image fusion. Those methods significantly improve the fusion quality of medical images.

Although many medical fusion methods have been introduced in the literature, the fused image quality still needs further improvements. Particularly, in terms of Visual information fidelity for fusion (VIFF) which is very helpful in supporting doctors and radiologists in the visual analysis of medical images, the latest result is 0.8169 as proposed in [10]. In this paper, we propose a new method for improving the visual information fidelity of the fused medical image. The main points of our method are as follows:

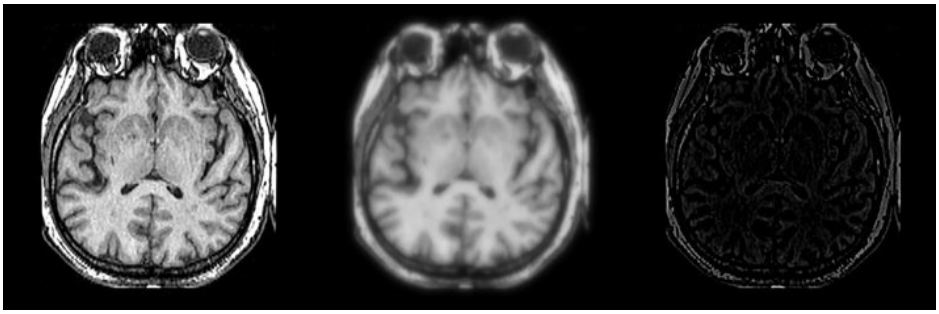

Figure 2: Illustration for the two-scale image decomposition: an input image (left) is decomposed into a base layer (middle) and a detail layer (right).

- The use of the Gaussian blur filter to create a gradual smoothing for the base layers of the input images.
- From the input images, the utilization of the Robinson compass operator to extract edge features for building rules to fuse the detail layers.

The organization of this paper is structured as follows. Section 2 presents foundation concepts such as contrast limited adaptive histogram equalization, Gaussian blur filter, YCbCr color space conversion, Robinson compass operator, and the proposed method for creating the fused image. The experiments and evaluation of the proposed method are presented in Section 3. Section 4 demonstrates the conclusion and some future directions of this work.

2. METHODS

2.1. Gaussian-blur filter two-scale image decomposition (GBF-TSID)

There are many different methods to perform image decomposition such as multi-scale transformation [14], sparse representation [15], and two-scale transformation [11]. Among the existing ones, two-scale image decomposition (TSID) methods (Fig. 2) are widely used in many research works for medical image fusion such as two-scale using Discrete wavelet transform (DWT) [11, 12], Fast fourier transform (FFT) [9, 10], or Gaussian Blur filter (GBF) [18]. In this section, we present the use of a Gaussian blur filter to perform the TSID of an input image (I) into two parts, called the base layer (I^b) and the detail layer (I^d). The base layer demonstrates the large-scale deviation or general features of the image while the detail layer contains small-scale variations or detailed information of the image. We chose GBF for TSID since it is efficiently used in other research works in medical image fusion [18].

To calculate I^b from the input image I, we perform a convolution operation on each pixel of the input image using a Gaussian filter G of the kernel size 5-by-5 as follows

$$G = \frac{1}{330}\begin{bmatrix} 1 & 4 & 7 & 4 & 1 \\ 4 & 20 & 33 & 20 & 4 \\ 7 & 33 & 54 & 33 & 7 \\ 4 & 20 & 33 & 20 & 4 \\ 1 & 4 & 7 & 4 & 1 \end{bmatrix}.$$

In Gaussian blur, the standard deviation σ of the Gaussian distribution controls the spread or width of the Gaussian curve. Increasing σ leads to a wider Gaussian curve,

intensifying the blur effect and increasing the effect of close pixels on the central pixel during blurring. On the contrary, reducing σ results in a narrower Gaussian curve, leading to a less pronounced blur effect. In this work, a standard deviation of 1 is used to have a standard Gaussian curve when performing TSID of the input images.

Subsequently, the detail layer I^d is deduced using the following suppression approach

$$I^d = I - I^b. \tag{1}$$

2.2. Robinson compass operator (RCO)

Edge detection holds significant importance for extracting features relevant to shape analysis, especially in medical imaging. Different compass operators are used in medical image fusion such as Kirsch [9] and Prewitt [10]. In this work, we employ the Robinson compass operator for edge detection of the input images. We chose the Robinson operator due to its ability to identify the highest edge strength along eight compass directions. The used eight Robinson compass masks are presented in Table 1.

Table 1: Illustration for 8 Robinson compass masks

$$\text{R1} = \begin{bmatrix} -1 & 0 & 1 \\ -2 & 0 & 2 \\ -1 & 0 & 1 \end{bmatrix} \quad \text{R2} = \begin{bmatrix} 0 & 1 & 2 \\ -1 & 0 & 1 \\ -2 & -1 & 0 \end{bmatrix} \quad \text{R3} = \begin{bmatrix} 1 & 2 & 1 \\ 0 & 0 & 0 \\ -1 & -2 & -1 \end{bmatrix} \quad \text{R4} = \begin{bmatrix} 2 & 1 & 0 \\ 1 & 0 & -1 \\ 0 & -1 & -2 \end{bmatrix}$$

$$\text{R5} = \begin{bmatrix} 1 & 0 & -1 \\ 2 & 0 & -2 \\ 1 & 0 & -1 \end{bmatrix} \quad \text{R6} = \begin{bmatrix} 0 & -1 & -2 \\ 1 & 0 & -1 \\ 2 & 1 & 0 \end{bmatrix} \quad \text{R7} = \begin{bmatrix} -1 & -2 & -1 \\ 0 & 0 & 0 \\ 1 & 2 & 1 \end{bmatrix} \quad \text{R8} = \begin{bmatrix} -2 & -1 & 0 \\ -1 & 0 & 1 \\ 0 & 1 & 2 \end{bmatrix}$$

2.3. Contrast limited adaptive histogram equalization (CLAHE)

In medical imaging, histogram equalization techniques are used to enhance the contrast of the input medical images [20, 21]. In this section, we present the CLAHE algorithm which is a variant of adaptive histogram equalization for reducing amplification of noise in the images. The main idea behind CLAHE involves dividing an image into smaller blocks and applying histogram equalization independently to each block. By constraining the contrast enhancement within these local regions and utilizing adaptive mechanisms, CLAHE prevents the global amplification of noise that can occur when using traditional equalization methods.

Let I be the input image, and I_{CLAHE} be the output image after applying the CLAHE algorithm. The CLAHE formula can be represented as

$$I_{\text{CLAHE}}(x, y) = \text{Interpolate}\left(\text{Clip}\left(\text{Equalize}(I_{\text{block}})\right)\right),$$

where I_{block} is the intensity values of the pixels within a block centered at (x, y).

2.4. YCbCr color space

There exist different color models to perform color space conversion in medical image fusion such as HSV [22], YUV [23], and YCbCr [10]. In this section, YCbCr color space is chosen since it is efficiently used in medical image fusion by other researchers in the literature [10]. The main idea of YCbCr space is the separation of luminance component (Y)

from chrominance components (Cb, Cr). Separation allows independent image processing methods, which is very helpful in enhancing visual fusion quality.
The RGB-YCbCr color space conversion is presented as follows

$$\begin{bmatrix} Y \\ Cb \\ Cr \end{bmatrix} = \begin{bmatrix} 0.257 & 0.564 & 0.098 \\ -0.148 & -0.291 & 0.439 \\ 0.439 & -0.368 & -0.071 \end{bmatrix} \begin{bmatrix} R \\ G \\ B \end{bmatrix} + \begin{bmatrix} 16 \\ 128 \\ 128 \end{bmatrix}.$$

Conversely, the YCbCr-RGB conversion is computed as follows

$$\begin{bmatrix} R \\ G \\ B \end{bmatrix} = \begin{bmatrix} 1.164 & 0.000 & 1.596 \\ 1.164 & -0.392 & -0.813 \\ 1.164 & 2.017 & 0.000 \end{bmatrix} \begin{bmatrix} Y - 16 \\ Cb - 128 \\ Cr - 128 \end{bmatrix}.$$

2.5. The proposed method

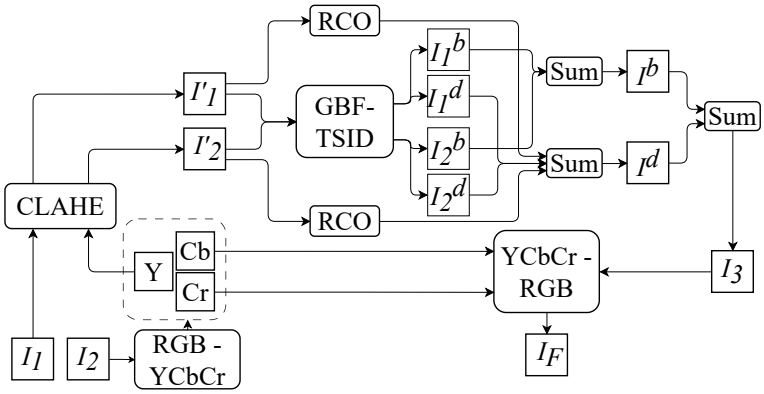

Figure 3: The diagram of the proposed method

The proposed method contains several steps as detailed in Fig. 3. Firstly, the medical color image is converted from RGB to YCbCr space. In the second step, the contrast of the medical images (the gray one and the obtained Y channel of the color one) is enhanced using the CLAHE algorithm. Then, a Gaussian-blur filter is implemented to split the enhanced images into the base and detail layers, and the edge features of the enhanced images are extracted using the Robinson compass operator (RCO). After that, we add two distinct detail layers and the extracted features to obtain a composite detail layer. For the composite base layer, it is created by summing two distinct base layers. Finally, the fused image is calculated by adding the composite base and detail layers together. This grayscale fused image is finally combined with the original Cr and Cb channels and transformed back to RGB to create the fused output image. The detail of the proposed method is presented in Algorithm 1.

3. EVALUATION

3.1. Evaluation metrics

There are many objective metrics to evaluate the quality of the used images. We use five different objective metrics in this paper: Average information of an image (Entropy or EN) [24]; Difference between the two input images and the fused image (Overall cross

Algorithm 1: The proposed method

Input : I_1 and I_2: grayscale and color medical image.s
Output: Fused image I_F in RGB format

Step (i): Convert the color medical image I_2 to YCbCr color space;
$(Y, Cb, Cr) = \text{RGB\_YCbCr}(I_2)$.

Step (ii): Enhance the contrast of the grayscale image I_1 and the obtained Y channel from Step (i) using the CLAHE algorithm;
$I_1' = \text{CLAHE}(I_1)$, $I_2' = \text{CLAHE}(Y)$.

Step (iii): Extract edge features from I_1' and I_2' using RCO;
$E_1 = \text{RCO}(I_1')$, $E_2 = \text{RCO}(I_2')$.

Step (iv): Decompose two images I_1' and I_2' using GBF-TSID;
$(I_1^b, I_1^d) = \text{GBF\_TSID}(I_1')$;
$(I_2^b, I_2^d) = \text{GBF\_TSID}(I_2')$.

Step (v): Fuse base layers and detail layers to obtain I^b and I^d;
$I^b = I_1^b + I_2^b$;
$I^d = I_1^d + I_2^d + E_1 + E_2$.

Step (vi): Calculate the fused image in grayscale;
$I_3 = I^b + I^d$.

Step (vii): Convert I_3, Cb and Cr from YCbCr to RGB;
$I_F = \text{YCbCr\_RGB}(I_3, Cb, Cr)$.

entropy or OCE) [24]; Edge information preservation ($Q^{AB/F}$) [25]; Feature mutual information (FMI) [26]; Visual information fidelity for fusion (VIFF) [27]. Those metrics are chosen to measure the overall image clarity and visual fidelity in the fused image. Among the five metrics, the OCE value is lower means the image quality is better whereas, for the other four metrics (EN, $Q^{AB/F}$, FMI, and VIFF), the bigger value means that the image quality is higher.

3.2. Experimental setup

The dataset contains 180 medical images with the size of 256×256 pixels extracted from slices 50 to 79 of the MRI/PET image of a normal person[1]. These images include 60 MRI and PET images in the Transaxial axes (Set-T), 60 MRI and PET images in the Sagittal axes (Set-S), and 60 MRI and PET images in the Coronal axes (Set-C) used to evaluate fusion results.

To evaluate the performance of the proposed method, we select several popular two-scale image decomposition methods along with four edge detection techniques for the experiments. The decomposition methods include the Gaussian-blur filter (GBF), Fast Fourier transform (FFT), and Discrete wavelet transform (DWT) and the edge detectors are Canny, Kirsch,

[1]Obtained from http://www.med.harvard.edu/AANLIB

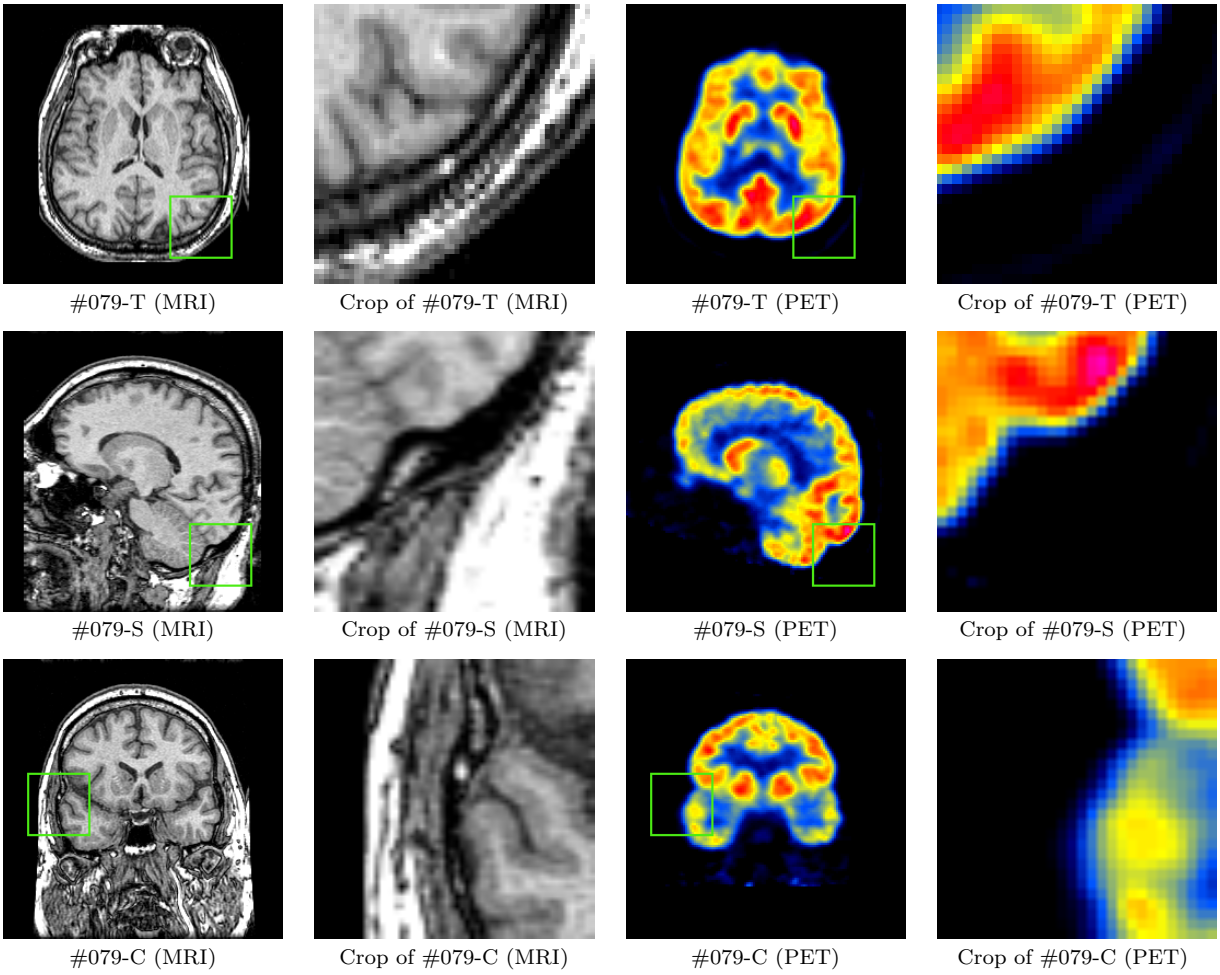

Figure 4: Different images to fuse in PET and MRI mediums and the corresponding extracted frames in the datasets Set-T (top row), Set-S (middle row), and Set-C (last row).

Prewitt, and Robinson operators. This paper evaluates the performance of our proposed method using five objective metrics: EN, OCE, $Q^{AB/F}$, FMI, and VIFF.

The experiments were performed using Python language and Matlab R2022a on a personal computer with Intel (R) Xeon (R) Gold 6133 CPU @ 2.50GHz, 32GB of RAM, NVIDIA GeForce RTX 3090 24 GB.

3.3. Results and discussion

From Table 2, our method yields the best results, in terms of OCE, FMI, and VIFF among the experimented popular approaches. Particularly, Table 3 shows that our method outperforms the state-of-the-art methods in medical image fusion in terms of visual information fidelity (0.9511 vs. 0.8169 as proposed in [10]). This indicates that our method performs well in transferring visual information fidelity of the input images to the fused image, which is an important feature of the fused image related to the human visual system for supporting doctors and radiologists in disease diagnosis and treatment.

Figure 4 shows examples of the three pairs (MRI/PET) of input images and the corre-

Table 2: Comparison of our proposed method and other popular approaches. The best results are highlighted in bold.

Dataset	Methods	EN	OCE	$Q^{AB/F}$	FMI	VIFF
Set-T	DWT Canny	5.2761	0.6033	0.4056	0.6835	0.5884
	DWT Kirsch	5.4880	0.5465	0.3719	0.8233	0.8965
	DWT Prewitt	5.5472	0.3998	0.4137	0.7705	0.4953
	DWT Robinson	5.4880	0.5461	0.3719	0.8233	0.8964
	FFT Canny	6.2843	0.4683	0.4178	0.6864	0.5953
	FFT Kirsch	6.4485	1.4745	0.4143	0.8149	0.8672
	FFT Prewitt	**6.4563**	0.4279	0.4416	0.7776	0.5043
	FFT Robinson	6.4445	1.4801	0.4137	0.8150	0.8671
	GBF Canny	5.4353	0.4747	0.4306	0.6906	0.6156
	GBF Kirsch	5.6492	0.1734	0.4367	0.8283	0.9508
	GBF Prewitt	5.5974	0.3810	**0.4681**	0.7807	0.5269
	GBF Robinson	5.6490	**0.1696**	0.4367	**0.8290**	**0.9511**
Set-S	DWT Canny	6.3622	1.3062	0.2431	0.6931	0.2530
	DWT Kirsch	6.4092	1.2576	0.2723	0.7709	0.3169
	DWT Prewitt	6.5038	1.2491	0.2067	0.7429	0.2745
	DWT Robinson	6.4091	1.2577	0.2722	0.7707	0.3169
	FFT Canny	6.9815	1.2901	0.2554	0.6783	0.2486
	FFT Kirsch	7.0602	1.2955	0.3851	0.7716	0.3181
	FFT Prewitt	**7.0706**	1.2164	0.2052	0.7405	0.2714
	FFT Robinson	7.0571	1.2941	0.3810	0.7709	0.3165
	GBF Canny	6.4748	0.4143	**0.5017**	0.6366	0.7883
	GBF Kirsch	6.4964	0.1636	0.4164	0.7650	0.8773
	GBF Prewitt	6.5448	0.4221	0.4430	0.7642	0.6683
	GBF Robinson	6.4940	**0.1586**	0.4137	**0.7805**	**0.8774**
Set-C	DWT Canny	5.8865	1.0965	0.2403	0.6937	0.2644
	DWT Kirsch	5.9633	1.0570	0.2348	0.7476	0.3018
	DWT Prewitt	6.0740	1.0073	0.1850	0.7216	0.2749
	DWT Robinson	5.9632	1.0571	0.2347	0.7474	0.3017
	FFT Canny	6.6189	1.0564	0.2473	0.6836	0.2544
	FFT Kirsch	**6.7324**	0.9859	0.3329	0.7429	0.2849
	FFT Prewitt	6.7288	0.9772	0.1771	0.7195	0.2655
	FFT Robinson	6.7286	0.9931	0.3286	0.7415	0.2830
	GBF Canny	5.9518	0.3424	**0.5008**	0.6411	0.8348
	GBF Kirsch	5.9788	0.0351	0.4342	0.7437	0.8850
	GBF Prewitt	6.0805	0.2424	0.4627	0.7423	0.6957
	GBF Robinson	5.9757	**0.0342**	0.4320	**0.7628**	**0.8878**

Table 3: Visual information fidelity of the proposed method and the latest approaches. The best result is highlighted in bold.

Methods	VIFF
GOA & FR-KCO [9]	0.7086
EOA & SLE_PCO [10]	0.8169
GBF Robinson on Set-T	**0.9511**
GBF Robinson on Set-S	0.8774
GBF Robinson on Set-C	0.8878

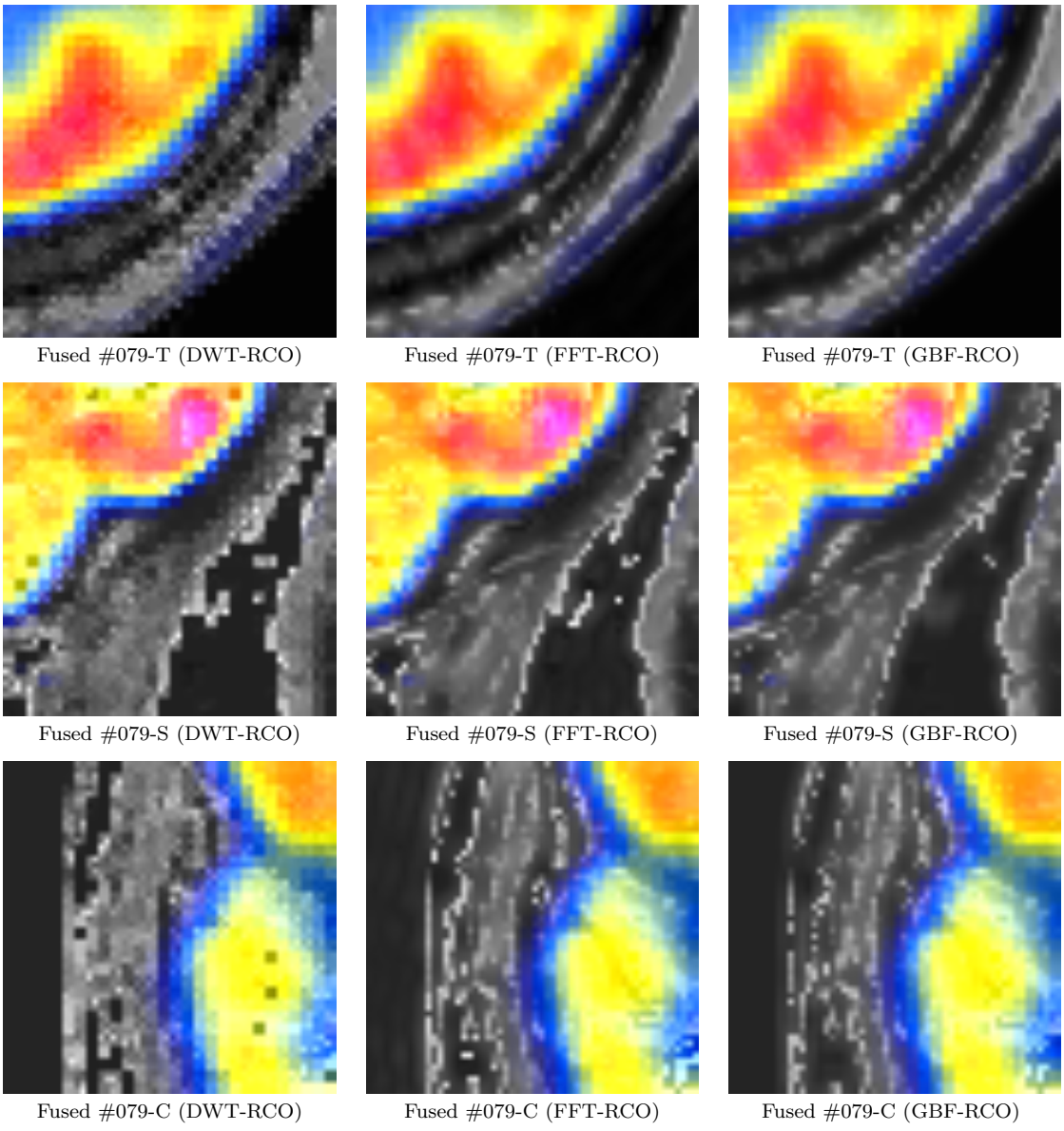

Fused #079-T (DWT-RCO) Fused #079-T (FFT-RCO) Fused #079-T (GBF-RCO)

Fused #079-S (DWT-RCO) Fused #079-S (FFT-RCO) Fused #079-S (GBF-RCO)

Fused #079-C (DWT-RCO) Fused #079-C (FFT-RCO) Fused #079-C (GBF-RCO)

Figure 5: Extracted frames of the fused images in the datasets Set-T (top row), Set-S (middle row), and Set-C (last row) using three experimented methods (DWT-RCO, FFT-RCO, and GBF-RCO).

sponding extracted frames in the datasets (Set-T, Set-S, Set-C) used in our experiments. The extracted frames of the fused images using three experimented methods (DWT-RCO, FFT-RCO, and GBF-RCO) on the three pairs (MRI/PET) of the input image are presented in Figure 5. It is easy to see that our method (GBF-RCO) shows substantial enhancements in the overall image clarity and visual fidelity in the fused image over the experimented methods.

4. CONCLUSION AND FUTURE WORKS

In this paper, a new method based on the Gaussian blur filter and Robinson compass operator is proposed to improve the visual information fidelity of the composite image in medical image fusion. Firstly, the CLAHE technique is applied to enhance the contrast of the input images. Then, a Gaussian blur filter is applied to split the input images into two distinct layers: base and detail ones. After that, the Robinson compass operator is employed to create the fusion rule of the detail layers. Finally, the decomposed base layers and the new detail layer are added together to form the final fused image.

The experiments were conducted on three datasets (Set-T, Set-S, and Set-C) using the popular two-scale image decomposition and edge detection approaches. We select five diffrent evaluation metrics (EN, OCE, $Q^{AB/F}$, FMI, and VIFF) to measure fusion quality. The evaluation shows that our method outperforms the latest approaches in bringing visual information fidelity of the input images to the fused image, which is helpful in supporting doctors and radiologists in the visual analysis of the medical images.

In the future, there are several potential directions to continue this work. Firstly, some optimization algorithms can be studied to improve the fusion step of the base layers. Next, more edge detection techniques such as transfer learning can be employed to form the efficient fusion rule of the detail layers. Last but not least, the study on improving input quality, such as contrast enhancement or noise removal, can also be a potential direction to continue this work.

ACKNOWLEDGMENT

This research was financially supported by the University of Science and Technology of Hanoi through project USTH.ICT.01/23.

REFERENCES

[1] A. P. James and B. V. Dasarathy, "Medical image fusion: A survey of the state of the art," *Information Fusion*, vol. 19, pp. 4–19, 2014. [Online]. Available: https://doi.org/10.1016/j.inffus.2013.12.002

[2] Y. Liu, L. Wang, J. Cheng, C. Li, and X. Chen, "Multi-focus image fusion: A survey of the state of the art," *Information Fusion*, vol. 64, pp. 71–91, 2020. [Online]. Available: https://doi.org/10.1016/j.inffus.2020.06.013

[3] S. Li, X. Kang, L. Fang, J. Hu, and H. Yin, "Pixel-level image fusion: A survey of the state of the art," *Information Fusion*, vol. 33, pp. 100–112, 2017. [Online]. Available: https://doi.org/10.1016/j.inffus.2016.05.004

[4] B. Meher, S. Agrawal, R. Panda, and A. Abraham, "A survey on region based image fusion methods," *Information Fusion*, 48:119–132, 2019. [Online]. Available: https://doi.org/10.1016/j.inffus.2018.07.010

[5] J. Fu, W. Li, J. Du, and B. Xiao, "Multimodal medical image fusion via laplacian pyramid and convolutional neural network reconstruction with local gradient energy strategy," *Computers in Biology and Medicine*, vol. 126, 2020. [Online]. Available: https://doi.org/10.1016/j.compbiomed.2020.104048

[6] Z. Wang, Z. Cui, and Y. Zhu, "Multi-modal medical image fusion by laplacian pyramid and adaptive sparse representation," *Computers in Biology and Medicine*, 123:103823, 2020. [Online]. Available: https://doi.org/10.1016/j.compbiomed.2020.103823

[7] S. Yang, M. Wang, L. Jiao, R. Wu, and Z. Wang, "Image fusion based on a new contourlet packet," *Information Fusion*, vol. 11, no. 2, pp. 78–84, 2010. [Online]. Available: https://doi.org/10.1016/j.inffus.2009.05.001

[8] X. Liu, W. Mei, and H. Du, "Multi-modality medical image fusion based on image decomposition framework and nonsubsampled shearlet transform," *Biomedical Signal Processing and Control*, vol. 40, pp. 343–350, 2018. [Online]. Available: https://doi.org/10.1016/j.bspc.2017.10.001

[9] P.-H. Dinh, "A novel approach based on grasshopper optimization algorithm for medical image fusion," *Expert Systems with Applications*, vol. 171, 2021. [Online]. Available: https://doi.org/10.1016/j.eswa.2021.114576

[10] P.-H. Dinh, "Multi-modal medical image fusion based on equilibrium optimizer algorithm and local energy functions," *Applied Intelligence*, vol. 51, no. 11, pp. 8416–8431, 2021. [Online]. Available: https://doi.org/10.1007/s10489-021-02282-w

[11] V. Bhavana and H. Krishnappa, "Multi-modality medical image fusion using discrete wavelet transform," *Procedia Computer Science*, vol. 70, pp. 625–631, 2015. [Online]. Available: https://doi.org/10.1016/j.procs.2015.10.057

[12] W. Tan, H.-x. Zhou, Y. Yu, J. Du, H. Qin, Z. Ma, and R. Zheng, "Multi-focus image fusion using spatial frequency and discrete wavelet transform," in *AOPC 2017: Optical Sensing and Imaging Technology and Applications*, volume 10462, pages 1215–1225. SPIE, 2017. [Online]. Available: https://doi.org/10.1117/12.2285561

[13] S. Maqsood and U. Javed, "Multi-modal medical image fusion based on two-scale image decomposition and sparse representation," *Biomedical Signal Processing and Control*, vol. 57, 2020. [Online]. Available: https://doi.org/10.1016/j.bspc.2019.101810

[14] Y. Liu, S. Liu, and Z. Wang, "A general framework for image fusion based on multi-scale transform and sparse representation," *Information Fusion*, vol. 24, pp. 147–164, 2015. [Online]. Available: https://doi.org/10.1016/j.inffus.2014.09.004

[15] D. S. Shibu and S. S. Priyadharsini, "Multi scale decomposition based medical image fusion using convolutional neural network and sparse representation," *Biomedical Signal Processing and Control*, vol. 69, 2021. [Online]. Available: https://doi.org/10.1016/j.bspc.2021.102789

[16] P.-H. Dinh, "A novel approach based on three-scale image decomposition and marine predators algorithm for multi-modal medical image fusion," *Biomedical Signal Processing and Control*, vol. 67, 2021. [Online]. Available: https://doi.org/10.1016/j.bspc.2021.102536

[17] P.-H. Dinh, "An improved medical image synthesis approach based on marine predators algorithm and maximum gabor energy," *Neural Computing and Applications*, vol. 34, no. 6, pp. 4367–4385, 2022. [Online]. Available: https://doi.org/10.1007/s00521-021-06577-4

[18] P.-H. Dinh and N. L. Giang, "Medical image fusion based on transfer learning techniques and coupled neural p systems," *Neural Computing and Applications*, vol. 36, no. 8, pp. 4325–4347, 2024. [Online]. Available: https://doi.org/10.1007/s00521-023-09294-2

[19] O. C. Do, C. M. Luong, P.-H. Dinh, and G. S. Tran, "An efficient approach to medical image fusion based on optimization and transfer learning with vgg19," *Biomedical Signal Processing and Control*, vol. 87, 2024. [Online]. Available: https://doi.org/10.1016/j.bspc.2023.105370

[20] N. Salem, H. Malik, and A. Shams, "Medical image enhancement based on histogram algorithms," *Procedia Computer Science*, vol. 163, pp. 300–311, 2019. [Online]. Available: https://doi.org/10.1016/j.procs.2019.12.112

[21] E. S. Gupta and S. S. Kang, "Image enhancement of medical images using curvelet and rayleigh clahe," *IOSR Journal of Computer Engineering*, vol. 20, pp. 69–80, 2018. [Online]. Available: 10.9790/0661-2003046980

[22] X. Jin, G. Chen, J. Hou, Q. Jiang, D. Zhou, and S. Yao, "Multimodal sensor medical image fusion based on nonsubsampled shearlet transform and s-pcnns in hsv space," *Signal Processing*, vol. 153, pp. 379–395, 2018. [Online]. Available: https://doi.org/10.1016/j.sigpro.2018.08.002

[23] Y. Liu, D. Zhou, R. Nie, R. Hou, Z. Ding, Y. Guo, and J. Zhou, "Robust spiking cortical model and total-variational decomposition for multimodal medical image fusion," *Biomedical Signal Processing and Control*, vol. 61, 2020. [Online]. Available: https://doi.org/10.1016/j.bspc.2020.101996

[24] Q.-g. Miao, C. Shi, P.-f. Xu, M. Yang, and Y.-b. Shi, "A novel algorithm of image fusion using shearlets," *Optics Communications*, vol. 284, no. 6, pp. 1540–1547, 2011. [Online]. Available: https://doi.org/10.1016/j.optcom.2010.11.048

[25] C. S. Xydeas and V. Petrovic, "Objective image fusion performance measure," *Electronics Letters*, vol. 36, no. 4, pp. 308–309, 2000. [Online]. Available: https://doi.org/10.1049/el:20000267

[26] M. B. A. Haghighat, A. Aghagolzadeh, and H. Seyedarabi, "A non-reference image fusion metric based on mutual information of image features," *Computers & Electrical Engineering*, vol. 37, no. 5, pp. 744–756, 2011. [Online]. Available: https://doi.org/10.1016/j.compeleceng.2011.07.012

[27] Y. Han, Y. Cai, Y. Cao, and X. Xu, "A new image fusion performance metric based on visual information fidelity," *Information Fusion*, vol. 14, no. 2, pp. 127–135, 2013. [Online]. Available: https://doi.org/10.1016/j.inffus.2011.08.002

Received on August 15, 2023
Accepted on April 04, 2024